J. Fluid Mech. (1989), *vol.* 198, *pp.* 1–26
Printed in Great Britain

On the breakdown of the wave packet trailing a turbulent spot in a laminar boundary layer

By A. GLEZER,† Y. KATZ‡ AND I. WYGNANSKI†‡

† Department of Aerospace and Mechanical Engineering, University of Arizona, Tucson, AZ 85721, USA

‡ Department of Fluid Mechanics and Heat Transfer, Tel-Aviv University, Tel-Aviv, Israel

(Received 11 February 1986 and in revised form 3 July 1987)

The evolution of two oblique wave packets trailing a transitional spot in a laminar boundary layer was investigated in order to determine the extent of the interaction between the packets and the spot. The experimental investigation, carried out on two slightly different laminar boundary layers characterized by Falkner–Skan constants of $\beta = 0$ and $\beta = 0.2$, revealed that very small pressure gradients can have significant effects on the stability of the laminar boundary layer and the rate at which it is contaminated by a turbulent spot. Some simple, novel statistical procedures for treating the data were developed and were used to accentuate the understanding of the physical processes governing transition to turbulence.

1. Introduction

The appearance of turbulent spots in a laminar boundary layer marks the final stages of the transition process the turbulence contained in these spots spreads in all directions, contaminating the laminar flow. Despite numerous investigations, the mechanism by which the spots entrain vortical fluid from within the boundary layer and irrotational fluid from above is still not well understood. The purpose of this study is to shed some light on the manner in which the spot destabilizes the surrounding laminar boundary layer and enables the propagation of turbulent interfaces into the non-turbulent fluid in both lateral and longitudinal directions.

The instability of the laminar boundary layer to small, random disturbances is well known. Amplification rates of plane Tollmien–Schlichting waves were verified experimentally by Schubauer & Skramstad (1948), and the evolution of a small-amplitude wave packet was examined theoretically by Gaster (1975) and experimentally by Gaster & Grant (1975). The nonlinear aspects of the phenomenon leading to rapid amplification and the eventual breakdown to turbulence remain an enigma to date. Klebanoff, Tidstrom & Sargent (1962), as well as Kovasznay, Komoda & Vasudeva (1962), triggered the breakdown of Tollmien–Schlichting waves by adding periodic spanwise irregularities, which generated streamwise vortices coupled with local inflexional velocity profiles. The velocity profiles created in this manner are inviscidly unstable, leading to rapid amplification of disturbances and the generation of turbulence. Kovasznay *et al.* mapped the vorticity contours associated with the initial breakdown to turbulence. In plan view, the shape of these contours resembles the boundaries of a turbulent spot.

Natural transition never occurs uniformly across the span because of small irregularities in the experimental apparatus. It is well known that the concentration of oscillating vorticity, at locations corresponding to the onset of turbulence, stems

from the very rapid amplification which occurs prior to breakdown. Turbulent spots are generated so swiftly that their evolution from a disturbance explicable by linear theory is only vaguely described in the literature. There are speculations suggesting that the evolution of shear waves may be entirely bypassed by some unknown, presumably inviscid, yet explosively amplified instability (Morkovin 1969).

The renewed interest in turbulent spots stems in part from the need to chart quantitatively the large coherent eddies in a fully developed turbulent boundary layer. This task still presents a major challenge to researchers in the field who, thus far, have only been able to provide some sketchy information. It has been demonstrated (Zilberman, Wygnanski & Kaplan 1976) that some portions of the spot retain their identity in a fully developed turbulent boundary layer over extremely long distances. The identifiable portions of the spot exhibit features in detailed agreement with the observed characteristics of the large coherent eddies in a turbulent boundary layer. Furthermore, flow visualization (Cantwell, Coles & Dimotakis 1978; Perry, Lim & Teh 1981) indicates that the large eddies within a turbulent spot are not different from the eddies existing in turbulent boundary layers. The eddies located near the boundaries of the spot, particularly at its spanwise extremities, might represent the most recent additions, which may therefore be more easily identifiable experimentally. These eddies may also be the product of the destabilization of the laminar boundary layer and, hence, correlated with a classical (presumably nonlinear) stability analysis.

An isolated spot, in the absence of a pressure gradient, is often trailed by two oblique wave packets whose frequency, wave speed, and amplitude distribution across the boundary layer correspond to Tollmien–Schlichting waves that had undergone the largest amplification (Wygnanski, Haritonidis & Kaplan 1979). These waves attain their maximum amplitude behind the 'wing-tips' of the spot, yet no waves were ever observed near the plane of symmetry. Since the group velocity of the wave packet is inclined to the plane of symmetry at an angle that is the same as the spreading angle of the spot itself, one can conclude that the two are correlated and that these waves are an important element in the transition process. This conclusion was reinforced by the breakdown of some of the waves in the packet and generation of new spots at high Reynolds numbers, thus setting up a chain reaction by which turbulence spreads in a laminar boundary layer. The interplay between a single spot and its trailing wave packet is further complicated by the fact that, at moderate Reynolds numbers, the distance separating the two increases with time while the spot travels downstream and retains its spreading rate in the spanwise and streamwise directions.

Gad-El-Hak, Blackwelder & Riley (1981) observed that the rate of growth of the spot in the lateral direction is an order of magnitude larger than its rate of growth normal to the solid surface. They argued that the turbulent region is bounded by irrotational fluid only in the direction normal to the surface and that the entrainment through this interface is governed by viscous forces, as observed by Corrsin & Kistler (1955). In the lateral and longitudinal directions, the spot is bounded by vortical fluid which is destabilized by disturbances induced by the spot. The destabilization of the laminar boundary layer is much more vigorous than the entrainment of irrotational fluid. Gad-El-Hak *et al.* verified these conjectures by flow visualization. They marked the initial patch of turbulence with dye and observed that the dye did not diffuse laterally at the same rate as the boundaries of the spot. The tagged turbulent fluid mixed rather slowly with the surrounding fluid, even when the latter was also turbulent. The hypothesis of destabilization does not agree with the classical

stability analysis because the wavelengths observed are shorter than predicted, while the amplification rates are greater than expected theoretically.

Chambers & Thomas (1983) attempted to establish the relationship between the spot and the wave packet trailing it by using flow visualization at a fairly low Reynolds number. They did not observe any breakdown of the wave packets into turbulence, thus questioning the universality of the earlier observations by Wygnanski *et al.* (1979). They suggested that *the wave packets are merely passive attendants to the spot.*

This paper describes some experiments linking the wave packet to the growth of the spot. It is a step in a continuing effort aimed at improving our understanding of the transition process and possibly exerting some measure of control over it. The measurements were made in the low-speed wind-tunnel facility at Tel-Aviv University at a free-stream velocity of 11.4 m/s, corresponding to Reynolds numbers based on the displacement thickness of the laminar boundary ranging from 1000 to 1500.

2. Experimental apparatus and data reduction

The basic experimental apparatus is not new. The facility and the ancillary equipment used in this experiment are described by Wygnanski, Sokolov & Friedman (1975). The spot was generated by a spark, approximately 2 mm in length, discharging in the spanwise direction near the surface of the plate and located 300 mm from its leading edge. The streamwise velocity component was measured with a rake of 10 hot wires spanning the height of the laminar boundary layer. Five hundred events, having a duration of 128 ms each, were recorded at every point. Measurements were taken at numerous streamwise stations at intervals of 5 mm in the spanwise direction extending beyond the wing-tip of the spot. The hot-wire rake, while butting the surface, positioned the nearest wire approximately 0.5 mm above the plate; the nominal spacing of the first six wires in the rake was also 0.5 mm (providing six data points in 3 mm). The data were ensemble-averaged, and curves were fitted to all the velocity profiles measured at each instant in time. This procedure yields a composite velocity field at any given (x, y)-coordinate as a function of the span z and the time t, often expressed as $U_1 t/x$.

Measurable pressure gradients on the surface of the plate were removed by adjusting the angle of attack of the plate and the top and bottom walls of the wind tunnel while monitoring the surface pressure with a Baratron pressure transducer or a Lambrecht manometer having an inclination of 25:1 (see also Wygnanski *et al.* 1975). Residual gradients were completely eliminated by making fine adjustments to the tunnel walls while monitoring the velocity profile until it fitted best the theoretical profile predicted by Blasius (i.e. Falkner–Skan constant $\beta = 0$). This was done by storing a family of Falkner–Skan profiles in the computer at increments of $\beta = 0.05$ and comparing each one individually with the measured velocity profile. A least-squares procedure was used to determine which value of β fitted the experimental results best. An acceptable level of standard deviation between the theoretical and the measured profiles was 1%. It was found that minute pressure gradients, unmeasurable by conventional means, could easily affect the shape of the velocity profile and significantly change the value of β.

The turbulent intensity of the streamwise velocity component, defined in the classical manner by

$$\overline{u'^2} = \lim_{T\to\infty} \frac{1}{T} \int_0^T (U - \bar{U})^2 \, \mathrm{d}t \tag{2.1}$$

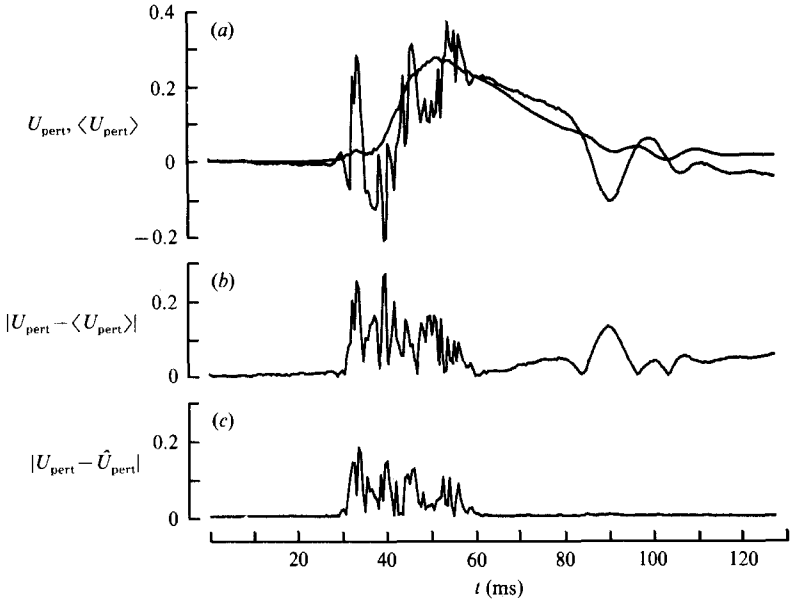

FIGURE 1. A comparison between a conventionally defined turbulence signal, (2.2), and a 'true' turbulence signal.

(where U is the instantaneous velocity, $\bar{U}$ is the mean velocity, and T is the time of integration), may be extended to N non-stationary events whose overall duration is subdivided into 512 equal time intervals (e.g. Van Atta & Helland 1980; see also Antonia *et al.* 1981) by

$$\langle u'^2 \rangle_J = \frac{1}{N} \sum_{I=1}^{N} [U(I,J) - \langle U(I,J) \rangle]^2, \tag{2.2}$$

where $\langle U(I,J) \rangle$ represents an ensemble-averaged velocity, N is the number of realizations, and J represents the discretized time t. Equation (2.2) is rendered dimensionless with respect to the free-stream velocity by defining $U_{\text{pert}} = [U(I,J) - U_{\text{lam}}]/U_1$, while $\langle \hat{U}_{\text{pert}} \rangle$ is the ensemble average of this quantity. Sample data of U_{pert} and $\langle U_{\text{pert}} \rangle$ are plotted in figure 1 (*a*), while the absolute value $|U_{\text{pert}} - \langle U_{\text{pert}} \rangle|$ is plotted in figure 1 (*b*).

In order to avoid errors arising from averaging over spots of different sizes, shapes and celerities, a different scheme for calculating the intensity of turbulent fluctuations was devised by replacing $\langle U(I,J) \rangle$ with $\hat{U}(I,J)$, a pseudo-mean velocity of *each* realization. This 'mean' may be thought of as the line that an experienced person would draw on the plot of a velocity trace resulting from the passage of an individual spot. Since the data are not stationary, a simple filter may not provide this result.

$\hat{U}(I,J)$ was computed by a running-average technique,

$$\hat{U}(I,J) = \frac{1}{2W_2+1} \sum_{K=J-W_2}^{J+W_2} U(I,K),$$

with a variable time window, W_2. This is a double-pass scheme. A time window W_1 is selected in the first pass and is centred on successive data points. The mean time derivative,

$$\frac{\Delta U}{\Delta T}(I,J) \propto \frac{1}{2W_1+1} \sum_{K=J-W_1}^{J+W_1} |U(I,K) - U(I,K-1)|,$$

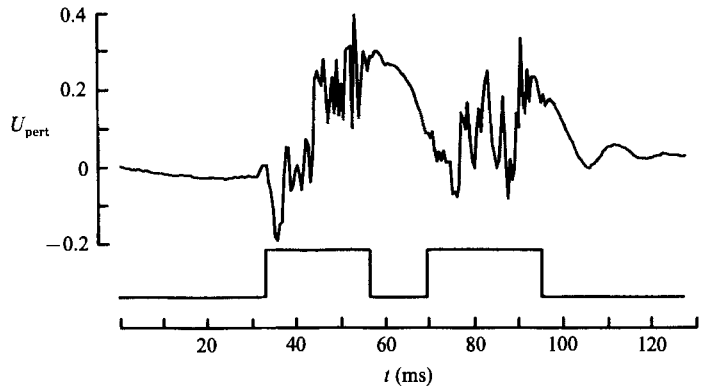

FIGURE 2. A typical 128 ms velocity record of the passage of the spot at $x_s = 810$ mm, $z = 85$ mm, and $y/\delta^* \approx 0.6$. Plotted below is a corresponding 'on–off' signal ($\epsilon/U_1 = 0.4\%$; see (2.3)).

of the velocity data within the window is computed for each centre point. In the second pass, the width of the window W_2 at each data point is varied proportionately to the time derivatives computed in the first pass ($W_2 \propto \Delta\hat{U}/\Delta T$), and the centre point is replaced by the mean of the data points included in the new window. The maximum width of the window in the turbulent zone encompassed 17 points, corresponding to 8 ms, while no averaging was necessary in the laminar boundary layer. A plot of $|U_{\text{pert}} - \hat{U}_{\text{pert}}|$ dubbed as the 'true' turbulent signal is shown in figure 1(*c*).

The presence of turbulence in the core of the spot is indicated by intermittency, ideally defined in terms of oscillating vorticity and therefore small-scale fluctuations. The intermittency in the present experiment was determined digitally from the streamwise component of velocity (Glezer & Coles 1988). Given a uniformly spaced time series $U(J)$, consider a least-squares fit of a straight line to three successive data points. The fitted line is parallel to a line passing through the first and third points but is displaced from it by a distance B. The r.m.s. deviation of the three points from the line is

$$\epsilon = \sqrt{2}B, \tag{2.3}$$

where

$$B = \tfrac{1}{2}\{U(J) - \tfrac{1}{3}[U(J-1) + U(J) + U(J+1)]\}.$$

Whenever ϵ exceeds a prescribed threshold level, the flow is assumed to be turbulent, setting the 'on–off' (telegraph) signal $G(J)$ to unity (figure 2). The intermittency γ_J is the ensemble average of this function generated by summing N events:

$$\gamma_J = \frac{1}{N}\sum_{I=1}^{N} G(I, J). \tag{2.4}$$

An effort was made to reduce the ambiguity in the mean quantities due to jitter in the arrival time and the duration of the spot. A simple ensemble-averaged velocity, conditionally triggered by the signal generator which also initiated the spot, was calculated first. Each event was correlated with the ensemble average and shifted in time until the deviation from the ensemble was minimized. The time shifts for each realization were recorded and used for averaging of all other quantities considered.

Although the time shifts reduce the exponential decay of the mean perturbation velocity and turbulent intensity observed near the leading and trailing interfaces,

they do not eliminate them entirely. The turbulence level near the interface may be better represented by the zone-averaged turbulence intensity (see Wygnanski & Fiedler 1970).

This quantity is defined by

$$\langle u_c'^2 \rangle_J = \left(\frac{1}{\gamma_J}\right)\frac{1}{N}\sum_{I=1}^{N} G(I,J)[U(I,J)-\hat{U}(I,J)], \tag{2.5}$$

where the function $G(I,J)$ is the 'on–off' signal defined above for the particular Ith event considered. Since $\langle u_c'^2 \rangle_J$ is an ensemble-averaged quantity which depends on the distance from the interface of the spot (i.e. on time), it is hereinafter referred to as a corrected turbulent intensity and not as a zone-averaged quantity as was done near the interface of a turbulent mixing layer (Wygnanski & Fiedler 1970).

3. Discussion of results

3.1. *Experiments at* $\beta = 0$

The first objective of this investigation was to reconcile the differences between the observations of Chambers & Thomas (1983) and the earlier observations of Wygnanski *et al.* (1979). The goal was therefore to establish the conditions leading to the breakdown of the waves following the spot and to determine whether the turbulence resulting from such a breakdown contributes to the growth of the spot.

Contours of the average velocity perturbation, $\langle U_{\text{pert}} \rangle$, resulting from the passage of the spot are shown in figure 3. These data were plotted in the (z,t)-plane approximately 1 mm above the surface (at $y/\delta^* \approx 0.6$). The positive contour levels vary between $+1\%$ and $+10\%$ at intervals of 1% relative to the undisturbed laminar velocity profile, while the negative contours (which are hatched in figure 3) vary between -0.5% and -2.5% at intervals of -0.5%. These measurements were taken at $x = 920$, 1110, and 1300 mm downstream of the leading edge, corresponding to $x_s = 620$, 810, and 1000 mm from the spark. Note that the data in figures 3–9 are plotted in *dimensional* variables, rather than in the traditional similarity variables, because of the breakdown of the waves and the formation of a new turbulent structure behind the spot.

The leading edge of the spot is easily recognizable by the steep gradients in the velocity perturbation levels. One may therefore choose either the 2% perturbation level (Coles & Barker 1975) or even the 10% level to mark the average location of the leading interface of the spot with reasonable accuracy. The trailing interface of the spot cannot be detected from these contour maps because, at this elevation above the surface, the non-turbulent velocity profile of the 'calmed region' (in the parlance of Schubauer & Klebanoff 1956) is similar to the turbulent velocity profile inside the spot. The shaded region corresponds to intermittency levels higher than 0.5. The wave packet is clearly visible on these plots (which is the reason for choosing this particular elevation in the first place). The waves attain their maximum amplitude at $z/x_s = 0.12$, and they decay or blend with the calmed region at smaller values of z/x_s. These results are in agreement with the results presented in figure 5 of Wygnanski *et al.* (1979). The amplitude and span of the waves diminish beyond $x_s > 900$ mm for reasons that will be discussed later. The waves originate from a region of lower velocity induced by the spot beyond its lateral tip. This region is more unstable to small disturbances than most of the surrounding laminar boundary layer

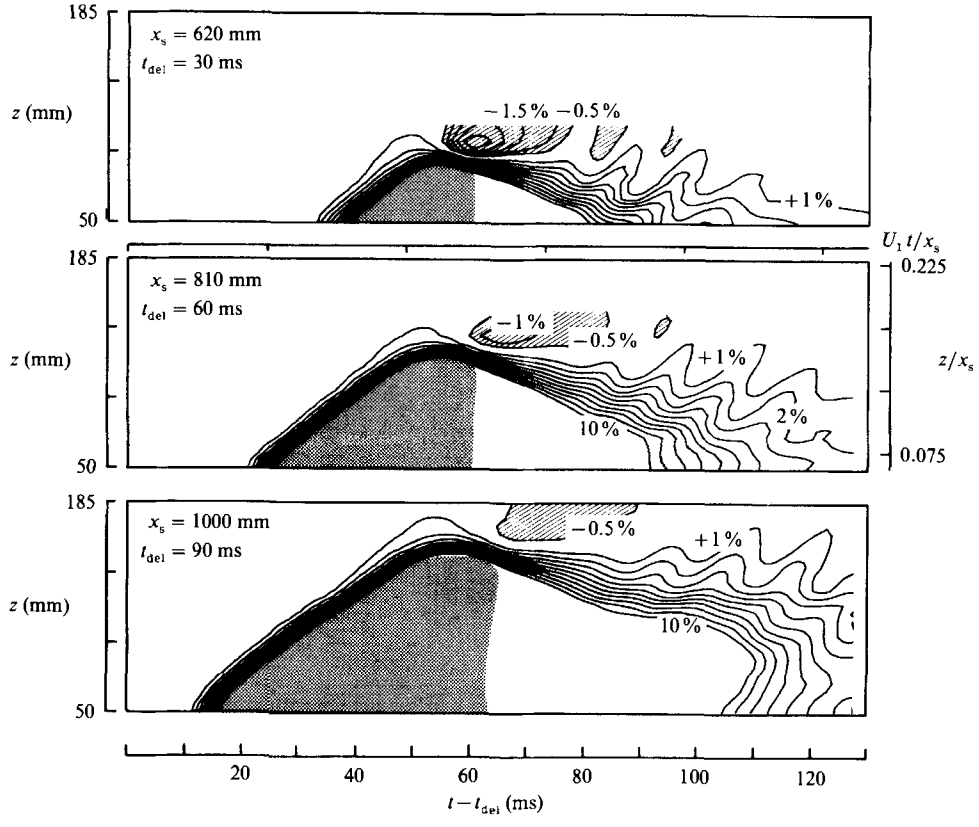

FIGURE 3. Contours of ensemble-averaged velocity perturbation measured at $y/\delta^* \approx 0.6$ and at x_s = 620 mm, 810 mm, and 1000 mm. Contour levels are 1% to 10% at intervals of 1%. Contour levels in the hatched areas are −0.5% to −2.5% at intervals of 0.5%. The shaded area indicates $\gamma > 50\%$.

(e.g. figure 17), and it moves with the tip of the spot. The velocity of the instability waves is generally lower and, consequently, the distance between the waves and the spot increases with time. The spot also induces an upwash along its entire leading edge (Wygnanski, Zilberman & Kaplan 1982), but this upwash is more confined to the immediate neighbourhood of the interface, thus making the resolution of an instability mechanism quite difficult. It is clear that the breakdown of the waves cannot be determined from ensemble-averaged mean velocity data, although the distorted contours of U_{pert} at x_s = 1000 mm may be indicative of this process.

The presence of an interface separating turbulent from non-turbulent fluid outside the main body of the spot can, in principle, serve as a measure for the breakdown of the waves. Such an interface is traditionally determined by a frequency-filtering operation forming an envelope to any rapidly fluctuating quantity and replacing this envelope by an 'on–off' signal. This procedure is not entirely objective as it requires an arbitrary determination of the threshold level that triggers the on–off signal. At a given location, some or all of the waves associated with a single event may or may not break down. Furthermore, when breakdown occurs, the duration of the turbulent region, its intensity, and the time of its appearance vary considerably from one realization to the next. As a result, the mapping of the new turbulent interface becomes somewhat dubious, and the largest values of the intermittency factor (i.e.

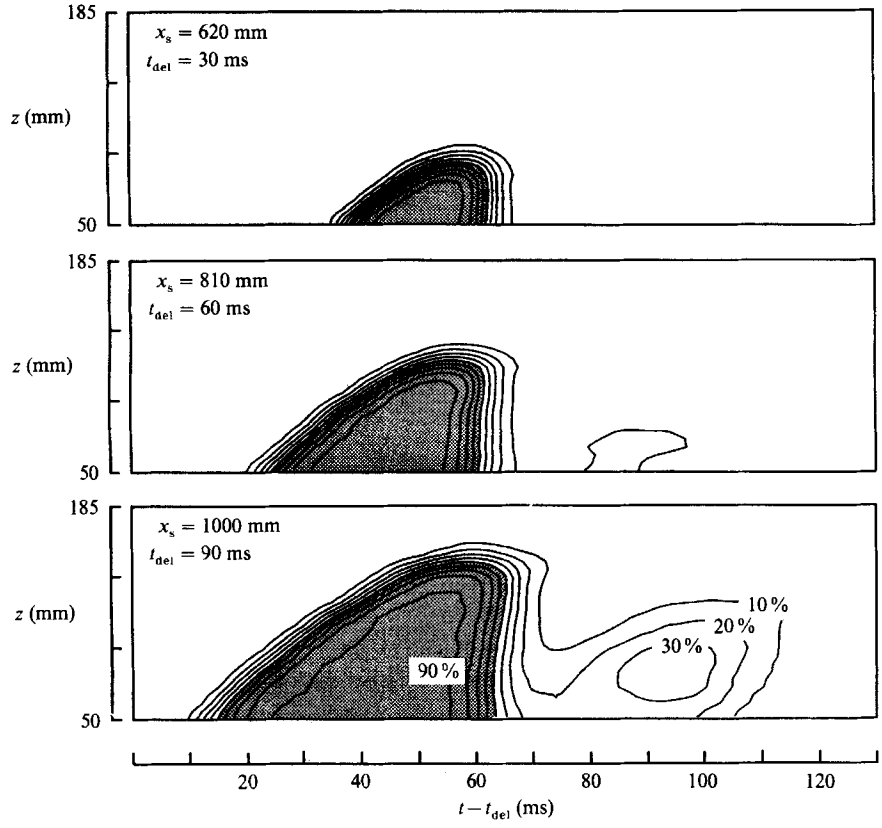

FIGURE 4. Spanwise distribution of intermittency contours at the same locations as shown in figure 3. Contour levels are 10%–100% at intervals of 10%. The shaded area indicates $\gamma > 50\%$.

the ensemble-averaged on–off signal) in a wave packet undergoing transition is a fraction which may never approach unity. The contour of $\gamma = 0.5$, which marks the average shape and size of the spot, no longer signifies the average location of the turbulent interface of the breaking wave packet. Nevertheless, the determination of γ is useful because it indicates the presence or absence of turbulence. The contours of intermittency shown in figure 4 (contour levels vary between 0.1 and 1.0 with increments of 0.1) indicate quite clearly that a turbulent region appears behind the spot at $x_s = 810$ mm, grows in size and partially amalgamates with the parent spot at $x_s = 1000$ mm.

The transition to turbulence of the wave packet and the destabilization process of the laminar boundary layer by the spot may be better represented and understood by means of the turbulent intensity. The conventionally defined turbulent intensity (equation (2.2)) includes the effects of jitter in the time of arrival of individual spots, as well as variations in their length, breadth, and shape at any streamwise location. All these effects contribute to the difference between the ensemble-averaged velocity and the instantaneous velocity, resulting in an *apparent turbulent intensity* near the leading and trailing interfaces of the spot. An example of the errors that might result from this procedure is shown in figure 1(*a*), in which one trace represents the ensemble-averaged perturbation velocity while the other trace superposed on it is the same perturbation velocity of a single realization; most of the fluctuating intensity plotted in figure 1(*b*) does not represent turbulence. In order to avoid these errors,

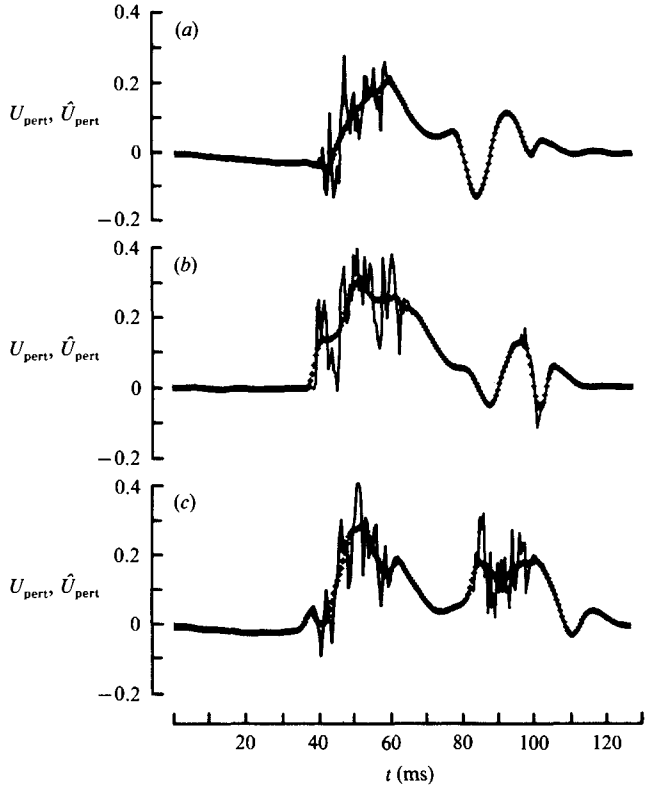

FIGURE 5. A detection of the breakdown to turbulence using the 'true' turbulence procedure.

a new scheme, described in §2, for calculating the intensity of the turbulent fluctuations was devised. The validity of the new scheme is demonstrated in figure 1(*c*). Representative temporal records of the perturbation streamwise velocity component, at various stages of wave breakdown, are shown in figure 5. The thin line, visible only when the flow was turbulent, represents the measured velocity and the + symbols correspond to the pseudo-'mean' (see §2) associated with the specific realizations shown. The waves depicted in figure 5(*a*) are not broken; they have a large amplitude comparable with the perturbation velocity produced by the spot. The waves shown in figure 5(*b*) just started to break down, while those shown in figure 5(*c*) formed a patch of turbulence. It is quite clear that the procedure described in §2 distinguishes between the low-frequency velocity oscillations associated with the passage of the spot or the waves and the high-frequency velocity oscillations signifying turbulence, yet it does not contribute to an erroneous turbulent intensity resulting from a phase or amplitude mismatch between the ensemble and the individual realizations.

Contours of the dimensionless turbulent intensity (u'/U_1) plotted at intervals of 1% in the (z, t)-plane are shown in figure 6. (The shaded area corresponds to a region in which $\gamma > 0.5$.) The gradual decrease in the turbulent intensity near the boundaries of the spot stems from averaging the data over spots of different dimensions and shapes; it does not represent a true gradient in the turbulent intensity within the spot. The high turbulent intensity observed near the wing-tip of the spot and near its leading edge at all values of x can only be explained by an enhanced turbulence production in this region.

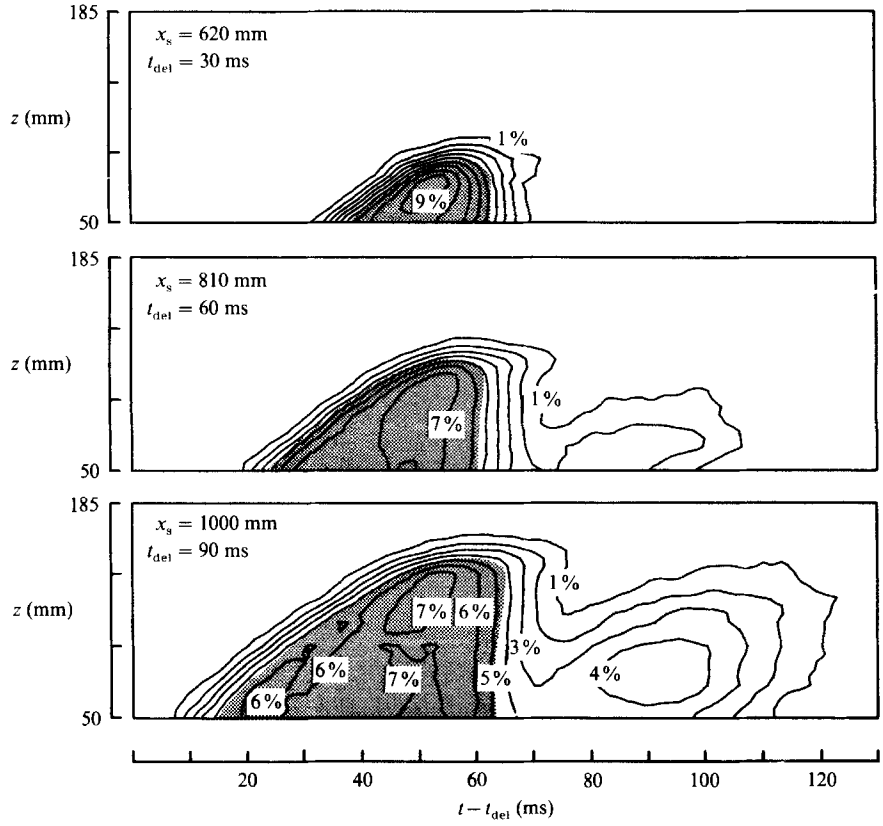

FIGURE 6. Spanwise distribution of 'true' r.m.s. contours at the same locations as shown in figure 3. Contour levels are 1%–10% at intervals of 1%. The shaded area indicates $\gamma > 50\%$.

Three contour maps of the ensemble-averaged turbulent intensity (u'/U_1) plotted in the (y,t)-plane for $z/x_s = 0.08$ are shown in figure 7. At $x_s = 620$ mm, no breakdown was observed since all the contours reside within a well-defined single structure. Farther downstream, the distribution of turbulent intensity is disfigured by a second turbulent region following the spot. At $x_s = 810$ mm, the intensity of the turbulence trailing the original spot is less than one-half of the intensity of turbulence within the spot but, at $x_s = 1000$ mm, this ratio is larger. The difference in the intensity levels inside the secondary turbulent region is, in part, an indication of the fraction of wave packets that break down at every location. The distribution of turbulent intensity within the spot changes with x as well. For example, the highest average turbulent intensity $(u'/U_1 > 10\%)$ measured at $x_s = 620$ mm occurs at a time corresponding to the passage of the ridge (or apex) of the spot at this (x,z)-coordinate but, at $x_s = 810$ mm and even more so at $x_s = 1000$ mm where the spot is much larger, the region of highest turbulent intensity (which is down to 7%) has shifted towards the leading interface. These contours provide additional evidence for the transition to turbulence occurring in the wave packet.

The observations made in the (z,t)-plane at $x_s = 1000$ mm (figure 6) also indicate that the highest turbulent intensities occur near the leading interface of the spot where the average intermittency is less than one. Since it is impossible to preselect spots of identical shapes and sizes, the structure of the flow near the interface is

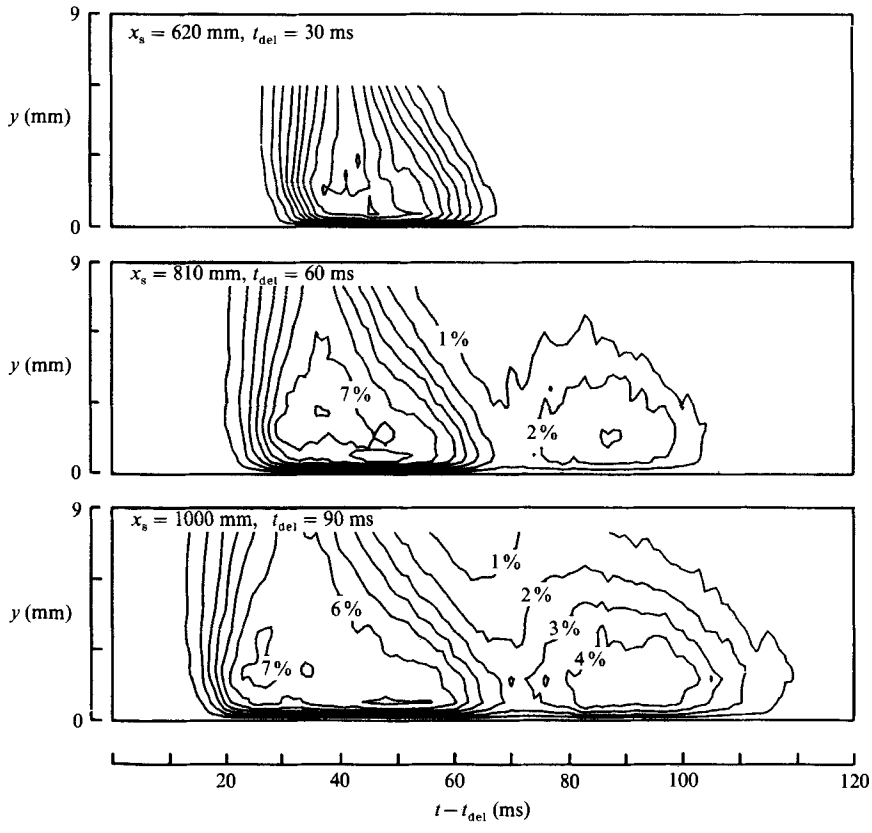

FIGURE 7. Contours of 'true' r.m.s. in the (y,t)-plane at $z/x_s = 0.08$. Contour levels are 1%–10% at intervals of 1%.

distorted by the averaging process. Thus, an averaging procedure that will take into account the differences among individual realizations is required. A representative turbulent-intensity distribution within an ensemble-averaged spot may be obtained from (2.5) which yields the equivalent of corrected zone-averaged data for non-stationary flows (figure 8). Since the present procedure of detecting turbulent intensity eliminated all fluctuations existing outside the turbulent zone, a simple division of the turbulent intensity by γ also gives a correct turbulent zone average, provided one does not carry the procedure to its limit (i.e. $\gamma \to 0$). In the contour plots shown in figures 8 and 9, the calculation procedure was stopped whenever $u'/U_1 < 2\%$. Setting the cutoff at different threshold levels of either γ or u'/U_1 did not alter the qualitative shape of the corrected turbulent-intensity contours. These contours not only reveal the existence of much sharper gradients near the boundaries of the spot, but also the existence of much higher levels of turbulent intensity near the boundaries. Although the precise ratio between the intensity of the turbulence near the boundary to the turbulent intensity in the centre of the spot depends to some extent on the method and the threshold levels used in computing the intermittency data, a variety of cross-checks verified the general validity of the results.

The corrected turbulent-intensity contours indicate an enhanced activity near the leading interface of the spot, where the average level is approximately twice as high as it is in the core of the spot. The highest corrected turbulence level recorded occurs

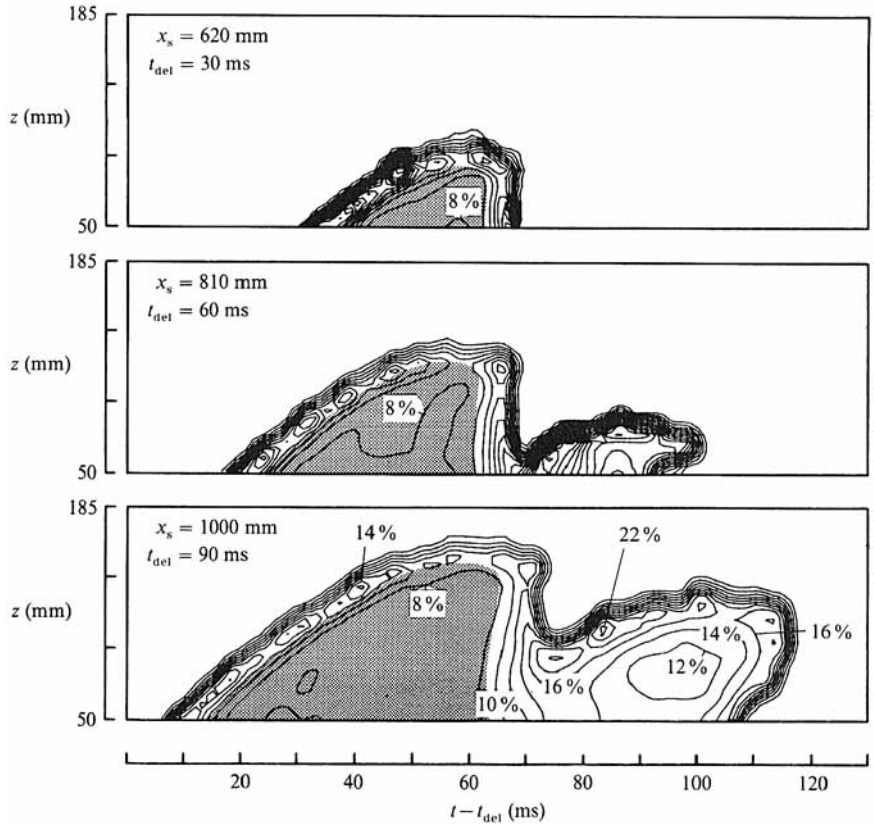

FIGURE 8. Contours of corrected r.m.s. in the (z,t)-plane at $x_s = 620$ mm, 810 mm, and 1000 mm at $y/\delta^* = 0.6$, $50 \leqslant z \leqslant 185$ mm. Contour levels are 2% to 32% at intervals of 2%. Some contour levels are marked for clarity. The shaded area indicates $\gamma > 50\%$.

in the juncture between the parent spot and the turbulent patch starting at $x_s =$ 810 mm. This location probably coincides with the portion of the crest of a wave that broke down first. As the turbulent patch increases, the turbulence level at its centre decreases and the boundary separating the parent spot from the patch is moved outward towards the tip of the parent spot. The highest level of corrected turbulent intensity at $x_s = 620$ mm (i.e. where the wave packet does not yet undergo transition to turbulence) occurs in the tip areas. The fact that the ensemble-averaged and the corrected turbulent intensities are lower near the centre of the spot than near its boundaries suggests that turbulence is generated along the peripheries of the spot. At this elevation from the surface, which is under the 'overhang' of the spot (i.e. the most forwardly protruding turbulent region in the leading interface of the spot), fluid is vigorously entrained through the leading interface (Wygnanski *et al.* 1979). It is possible that the laminar boundary layer in this region is highly destabilized by the presence of the leading edge of the spot. The level of turbulent intensity in flows undergoing transition is usually well above the level prevailing in fully developed turbulent flows (e.g. the turbulence level near the interface of a slug in transitional pipe flow; Wygnanski & Champagne 1973), and the peripheral area of the spot is no exception. This indicates that the leading edges of the patch and the parent spot are very active in destabilizing the surrounding laminar boundary layer, in spite of the

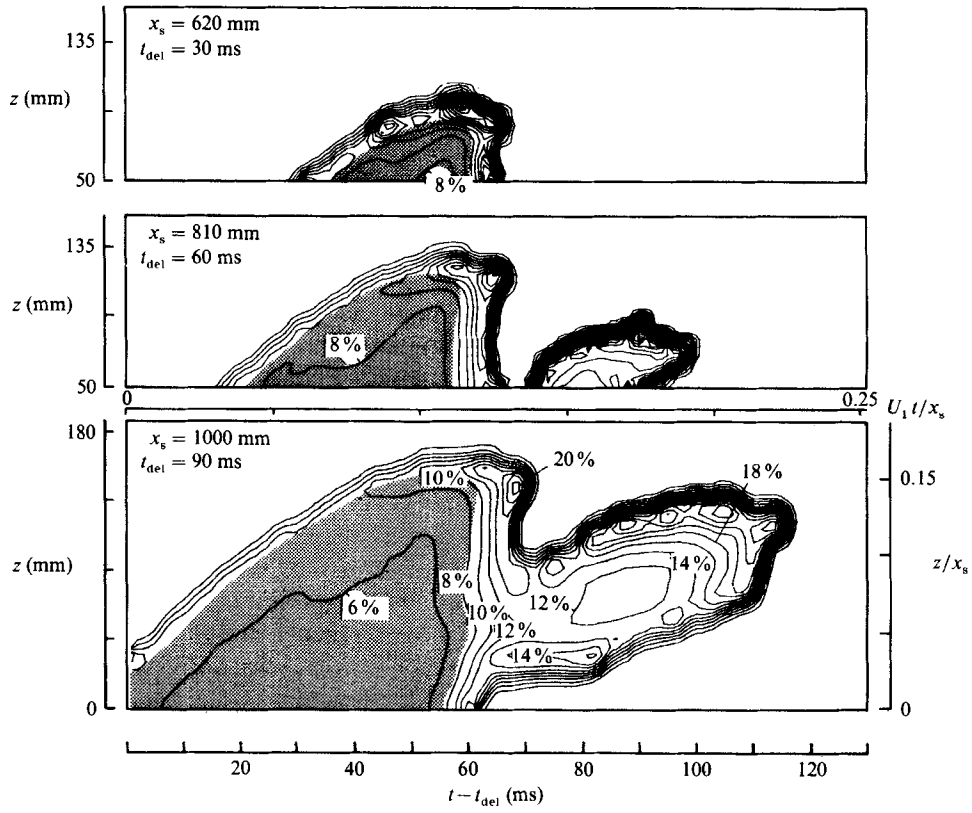

FIGURE 9. Contours of corrected r.m.s. in the (z,t)-plane corresponding to the location of the overhang of the spot ($y/\delta^* = 1.75$). At $x_s = 620$ mm and 810 mm, $50 \leqslant z \leqslant 135$; at $x_s = 1000$, $0 \leqslant z \leqslant 185$ mm. Contour levels are the same as in figure 8. The shaded area indicates $\gamma > 50\,\%$.

fact that entrainment considerations near the plane of symmetry suggest that most of the turbulent activity occurs at the trailing interface. Gad-El-Hak *et al.* (1981) also observed a strong destabilization of the laminar boundary layer under the 'overhang' of the leading interface.

Kovasznay *et al.* (1962) observed that the initial breakdown to turbulence in a boundary layer excited by a vibrating ribbon occurs at the outer part of the laminar boundary layer coinciding with the location of the overhang at $y/\delta^* = 1.75$. The shape of the leading edge of the spot (i.e. the presence of the overhang) may thus be related to the initial y-location of breakdown. The turbulent intensity and the contour map corresponding to $x_s = 1000$ mm is the only one that extends to the plane of symmetry (i.e. $z = 0$) and, consequently, this section is best suited for comparison between $y/\delta^* = 0.6$ and $y/\delta^* = 1.75$. The results indicate that the turbulent activity near the leading interface ceased at $y/\delta^* = 1.75$ (figure 9), while the turbulent intensity near the tip of the parent spot and the turbulent patch increased by at least 50% when compared with the data at $y/\delta^* = 0.6$ (figure 8). Since higher levels of turbulence occur near the tip of the spot at $y/\delta^* = 1.75$, one may suggest that the spot grows in the spanwise direction by breakdown of the waves originating in the low-velocity region at the tip. It is further conjectured that the spot grows in the streamwise direction by amplifying perturbations beneath the overhang.

The corrected turbulent intensity contours at the spanwise edge of the turbulent patch are wavy, in spite of the fact that neither the intermittency contours nor the ensemble-averaged turbulent-intensity contours exhibit such behaviour. The wavy pattern stems from the manner in which these contours cross one another. This occurs whenever a wave starts to break at some location along the crest (usually at a location at which the wave crest attained its highest amplitude) and the breakdown process progresses along the wave crest. This is analogous to the formation of surf in shallow-water waves. The intensity of turbulence at the location where breakdown first occurred increases with time, while the turbulent fluid is convected with the crest of the wave. The boundary at which turbulence is first observed (as identified by the on–off signal) moves along the wave crest and is therefore oblique to the steepest gradient of turbulent intensity. Whenever the results are ensemble-averaged, the borders of the turbulent region which form an acute angle with the turbulent-intensity contours are replaced by intermittency contours. The wavy contours at the extremities of the turbulent patch (whose characteristic timescale coincides with the period of the observed waves) and the associated high levels of the corrected turbulent intensity (figures 8 and 9) reflect the history of the wave packet's transition to turbulence. The similarities in the corrected turbulent-intensity contours at the tip of the spot and in the turbulent patch trailing the spot suggest that the breakdown of Tollmien–Schlichting waves is responsible for the propagation of turbulence in the transverse direction. The direct degeneration of the wave crests into turbulence was not observed in the tip region, perhaps because of the speed at which this process takes place in the present experiment.

It was shown (figures 7–9) that for $x_s > 620$ mm ($x = 920$ mm, corresponding to $Re_{\delta^*} = 1340$), some wave crests in the packet become turbulent, generating a new region which increases in size as it proceeds downstream. Since the laminar wave packet lags behind the spot, a separate turbulent patch in the shape of a small spot emerges upon breakdown upstream of the wing-tip of the parent spot (see also Wygnanski *et al.* 1979). However, in time, the leading edge of this turbulent patch accelerates, catching up with the trailing edge of the parent spot and slowly amalgamating with it.

One may attribute the change in the shape of the plan view of the spot with time or with increasing downstream distance to the amalgamation process occurring between the turbulent patch and the parent spot. In fact, a small spot is initially triangular in shape, having a straight trailing edge perpendicular to the direction of streaming (Matsui 1980; Gad-El-Hak *et al.* 1981; Chambers & Thomas 1983), while a large and mature spot has a more concave trailing interface resembling an arrowhead shape (Cantwell *et al.* 1978). The corrected turbulent-intensity contours which extend to the plane of symmetry of the spot (figure 9, $x_s = 1000$ mm) indicate that the 'calmed region' on the plane of symmetry is not affected initially by the new turbulent patch. However, the outer part of the calmed region is continuously contaminated by new turbulence generated by the breakdown of the waves. The corrected turbulent intensity inside the patch increases almost monotonically with increasing z, indicating that the waves keep breaking down at large z, while the 'oldest' turbulence in the patch resides closer to the plane of symmetry. When the experiment is carried out at a much higher free-stream velocity (i.e. 20 m/s; see Wygnanski *et al.* 1979), the turbulent patch retains its separate entity over larger streamwise distances, which may be attributed in part to more rapid convection of the spot relative to the waves.

3.2. *Experiments at* $\beta = 0.2$

The boundary layer in the experimental observations discussed above was marginally stable to small disturbances for $x_s < 350$ mm (corresponding to $Re_{\delta^*} = 500$). This resulted in an initial decay of the waves. Farther downstream, the boundary layer became unstable, causing amplification and eventual breakdown of the waves. Since the stability of the boundary layer to small disturbances is greatly affected by the pressure gradient (Wazzan, Okamura & Smith 1968), the same may hold for the amplification of the wave packet accompanying the spot. Some aspects of the experiment were therefore repeated in the presence of a *slightly favourable* pressure gradient for the purpose of delaying the breakdown process. The mean velocity profile was described by a Falkner–Skan parameter, $0.1 < \beta < 0.2$, which was still somewhat smaller than the β reported by Cantwell *et al.* (1978). The pressure differential required to produce this deviation from the Blasius velocity profile was immeasurably small [i.e. it could not be detected on the most sensitive scale of a Lambrecht manometer, implying that $\Delta p/(1/2(\rho U_1^2)) < 0.005$], *yet the critical Reynolds number increased from* 500 *at* $\beta = 0$ *to* 2800 *at* $\beta = 0.2$.

The average velocity perturbations resulting from the passage of the spot at $x_s = 620$ mm were compared for both values of β. The Reynolds number based on δ^* at that location was approximately 1200 and 1300 for $\beta = 0.2$ and $\beta = 0$, respectively; the laminar boundary layer therefore was stable for $\beta \geqslant 0.08$ and unstable at $\beta = 0$. The two spots and their accompanying wave packets are qualitatively similar, although the overall dimensions of the spot embedded in laminar boundary layer characterized by $\beta = 0.2$ were diminished by the favourable pressure gradient and the accompanying packets did not break down at comparable Reynolds numbers. Thus, there is no new turbulence introduced into the calmed region, unlike the case $\beta = 0$. Since no breakdowns of waves were observed, the conditions were deemed suitable for studying the behaviour of the wave packet, the establishment of its origin, and its possible link with the selective destabilization of the boundary layer in the vicinity of the tip of the spot.

A typical, ensemble-averaged, velocity record obtained beyond the tip of the spot at $x_s = 580$ mm, $y = 1$ mm, and $z = 90$ mm (figure 10; see also figure 4(*b*) of Wygnanski *et al.* 1979) resembles the velocity field associated with a Rankine vortex and indicates a reduction in velocity after the passage of the tip. The region of reduced velocity may be regarded as a 'moving generator' for the waves emanating from it. It is easy to analyse the characteristic parameters of the wave packet from the ensemble-averaged records, provided the averaging procedure does not obliterate the waves. Spectral analysis of the averaged data indicates that the predominant frequency of the waves in the packet varies between 80 and 100 Hz. In order to establish the relevance of these findings, a similar analysis was applied to the individual realizations. The signals were low-pass filtered, Fourier transformed, and hanned (see also Wygnanski *et al.* 1979). The resulting ensemble-averaged frequency of the waves was again determined to be in the range of 80–100 Hz. A schematic representation of the averaged wave packet in a coordinate system moving with the spot is shown in figure 11 for $600 < x_s < 720$ mm. The boundaries of the spot are represented in this figure by the contour of $\gamma = 0.5$, which is equivalent near the tip of the spot to a 5% level of 'true' turbulent intensity. The size of the tick-marks represents the local amplitude of the wave crest of the ensemble-averaged velocity signal. The waves extend in the spanwise direction beyond the boundaries of the spot, but they do not appear in the calmed region trailing the spot. At $x_s = 600$ mm,

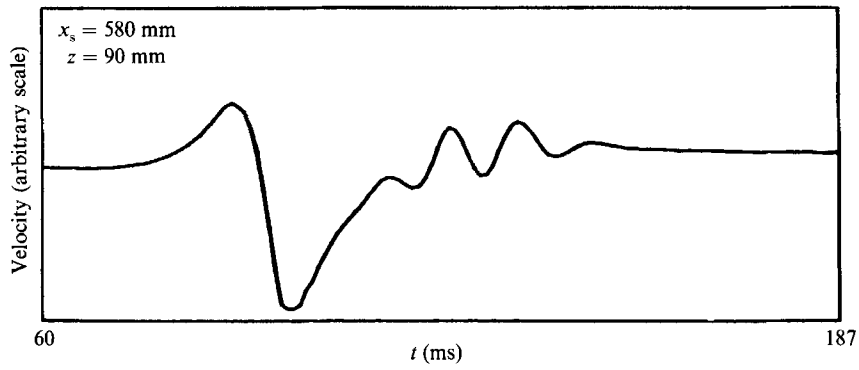

FIGURE 10. Ensemble-averaged velocity perturbation beyond the wing-tip of the spot.

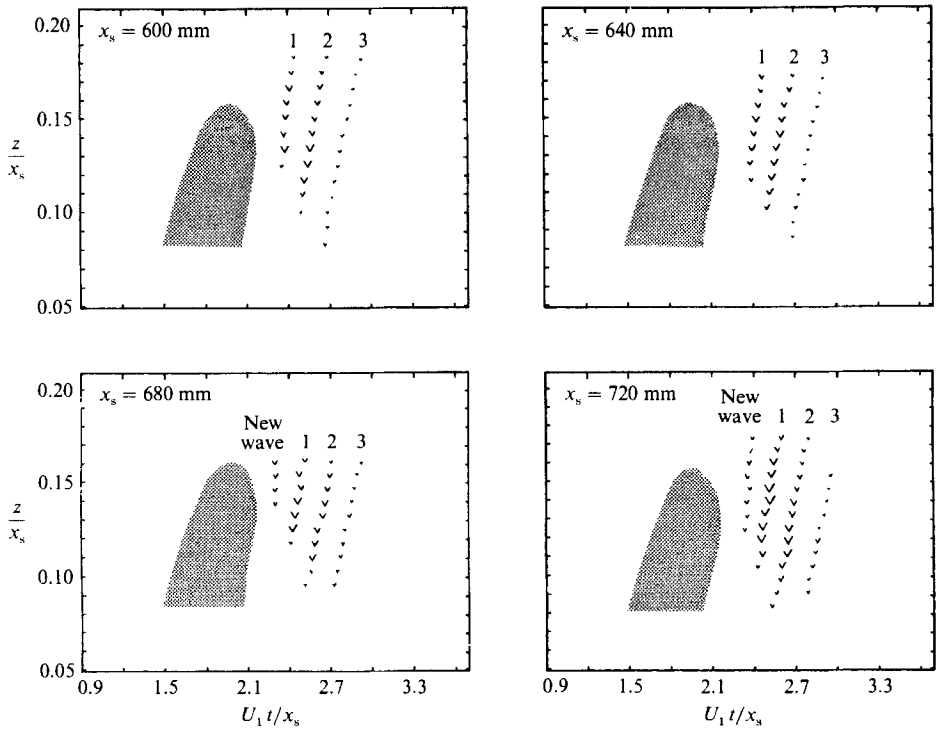

FIGURE 11. The location of the wave crests relative to the spot. The size of the symbol represents the amplitude of the crest.

only three waves crests are visible in the packet, but at $x_s = 680$ mm, a new wave crest emerged from the moving generator, increasing the number of crests in the packet to four. The maximum amplitude of wave 1 (closest to the trailing interface of the spot) in the packet is approximately doubled between $x_s = 580$ and $x_s = 740$ mm. The maximum amplitude of this wave crest propagates along the ray $z/x_s = 0.14$ which forms an angle of 8° with the plane of symmetry of the spot. The maximum amplitude of the second crest does not change with x_s over the range considered; it propagates along a ray defined by $z/x_s = 0.125$, therefore diverging from the plane of symmetry at a smaller angle of 7°. The maximum amplitude of the

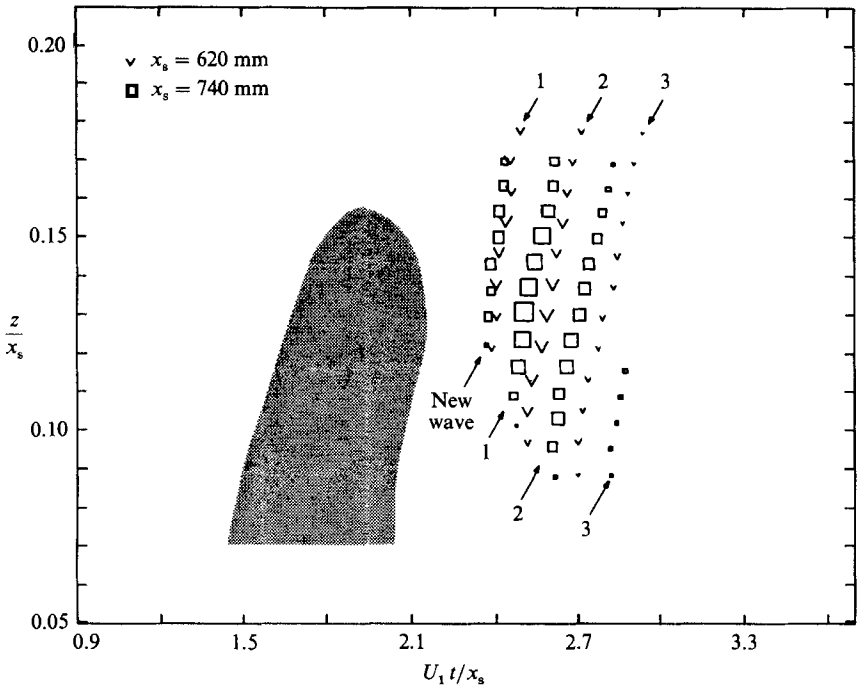

FIGURE 12. Superposition of the spot boundaries and the wave crests in dimensionless coordinates. The size of the symbol represents the amplitude of the wave crest.

third wave crest decays, while the corresponding maximum amplitude of the new wave crest increases rapidly with x.

In order to establish the relative position between the wave packet and the spot, the data acquired at $x_s = 620$ and $x_s = 740$ are superimposed on one figure (figure 12). The coordinates chosen for this purpose are $U_1 t/x_s$ and z/x_s because, in these coordinates, the boundaries of the spot remain invariant in the absence of breakdown. The 'new wave' seen at $x_s = 740$ replaced the location of wave 1 seen at $x_s = 620$, indicating that the gap between this wave crest and the trailing edge of the spot increases proportionally to x_s. The average streamwise component of the propagation velocity of the wave crest is $0.32U_1$, while the trailing interface of the spot at this y-location is convected downstream at $0.5U_1$. The wavelength between the crests of the packet, which is proportional to $U_1 t$ does not scale with x_s, therefore, in spite of the fact that wave 1 at $x_s = 620$ mm coincides with the 'new wave' at $x_s = 740$ mm (figure 12), the rest of the wave crests do not follow suit. The group velocity of the wave packet was calculated after fitting an envelope to the ensemble-averaged, hanned, and filtered velocity data (figure 13). The streamwise component of the group velocity measured between $x_s = 600$ mm and $x_s = 720$ mm at $z > 80$ mm is $0.35U_1$, and it diminishes to $0.3U_1$, closer to the plane of symmetry. The waves in the packet are essentially non-dispersive over the distance considered. Since the gap between the wave packet and the spot increases with x_s, the isolated packet does not contribute to the streamwise rate of growth of the spot in the given range of Reynolds numbers and a favourable pressure gradient. These might have been the experimental conditions investigated by Chambers & Thomas (1983). A possible explanation for the fact that Cantwell *et al.* (1978) did not observe the existence of

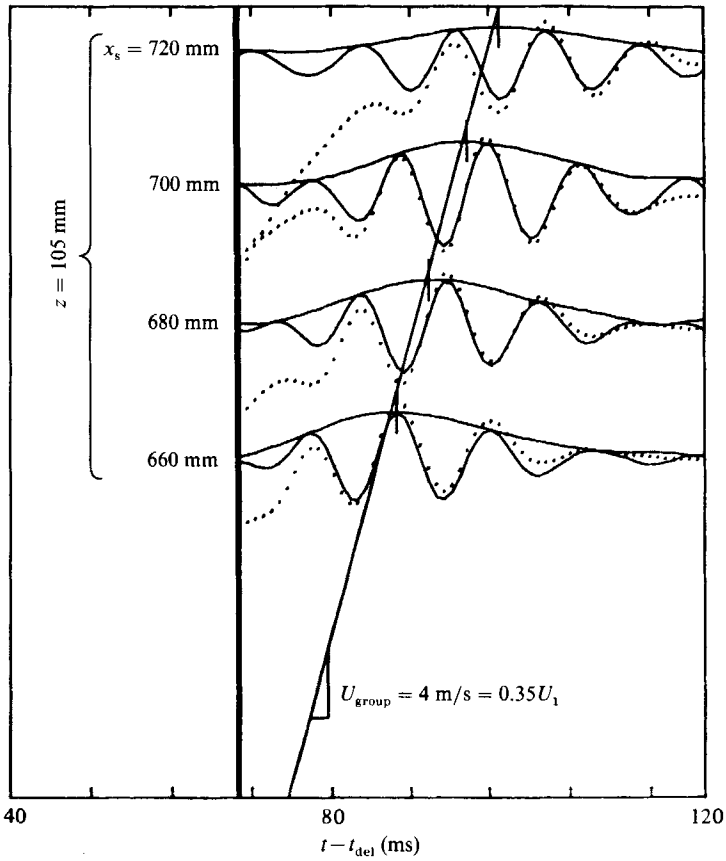

FIGURE 13. An example showing the determination of the group velocity of the packet. Dotted lines refer to the ensemble-averaged data, solid lines shows the hanned and filtered data. The time and x-location of the envelopes gives the streamwise component of the group velocity.

waves in their experiment may be attributed to the value of β that they reported (i.e. $\beta = 0.25$).

One may reconstruct the ensemble-averaged data in space at a given instant in time from the closely spaced measurements of velocity perturbation in the laboratory coordinates and therefore assess the geometric relationship between the spot and the wave packet. Velocity perturbation in the $x,z\,(580 < x_s < 700;\ 45 < z < 110)$-plane at a time corresponding to 144 ms after the initiation of the spot are shown in figure 14. At large absolute values of z, the wave crests and troughs are inclined to the plane of symmetry at an angle of 45°. The wave crests turn towards the spot at smaller values of z, and the resulting velocity perturbation associated with them should become more significant in the (y,z)-plane. The streamwise streaks observed in the calmed region following the spot (Gad-El-Hak *et al.* 1981) may be associated either with the turning of the waves or with remnants of longitudinal vortices present within the spot.

The change in the inclination angle of the averaged wave crests with decreasing z and the concomitant decrease in their amplitude raised the possibility that the averaging procedure might not have been physically meaningful. In order to resolve this question, the characteristics of the wave packet in each realization were

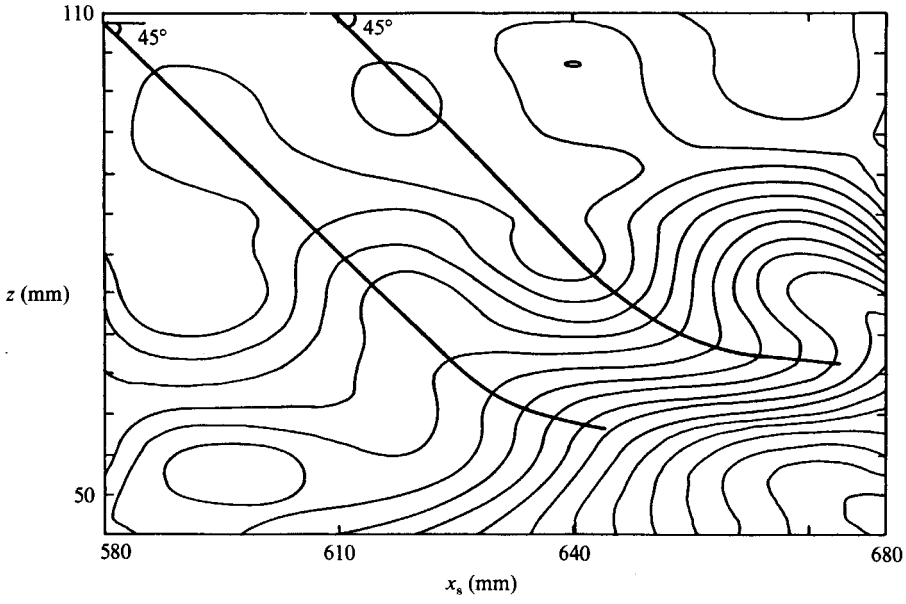

FIGURE 14. Contours of velocity perturbation in the (x, z)-plane at $t_s = 144$ ms. t_s is measured from the spark.

analysed. The velocity signal was low-pass filtered at 200 Hz, and the time of occurrence of each wave trough was determined, in addition to its amplitude relative to the surrounding crests. A representative sample of the results is shown in figure 15(*a–d*) for $\beta = 0.2$ and in figure 15(*e–g*) for $\beta = 0$. (These measurements were taken at $x_s = 620$ and $45 < z < 110$, i.e. between the first spanwise location at which waves have been observed and the maximum spanwise location at which the amplitude of the waves was still discernible.) The ensemble-averaged velocity perturbation is also shown on each of the plots. The histograms shown represent the time of occurrence of the wave troughs. All histograms show either 3 or 4 distinctive peaks, meaning that most of the wave packets contain 3 to 4 waves. The time of occurrence of these peaks coincides with the most probable time at which a trough occurs, and the 'steepness' of the peak represents the degree of repeatability of the events. Since these peaks do not overlap (i.e. the histogram drops to zero between adjacent peaks), the area under each peak divided by the total area represents the relative probability that a trough will occur during a prescribed time interval at a given location. At $z/x_s < 0.08$ or at $z/x_s > 0.16$, waves were only observed in less than 20% of the events, and clear wave crests surrounded by troughs on either side were even rarer. The resulting histograms which correspond to data collected at the outer spanwise region of the spot were poorly defined (see figure 15*d*). For $0.11 < z/x_s < 0.15$, the number of occurrences at which waves were observed was large, having a maximum of 75% of the total number of realizations at $z/x_s \approx 0.13$ for both values of β. The histograms corresponding to $0.11 < z/x_s < 0.15$ indicate that the average jitter in the time of arrival of the wave troughs (or crests) expressed by a standard deviation of each histogram is approximately 2 ms. The jitter in the arrival time of the leading interface of the spot at approximately the same location is also 2 ms (Zilberman 1981), indicating that the waves are triggered by the individual spots. Since the time interval between adjacent wave crests varies between 10 and 12 ms (corresponding

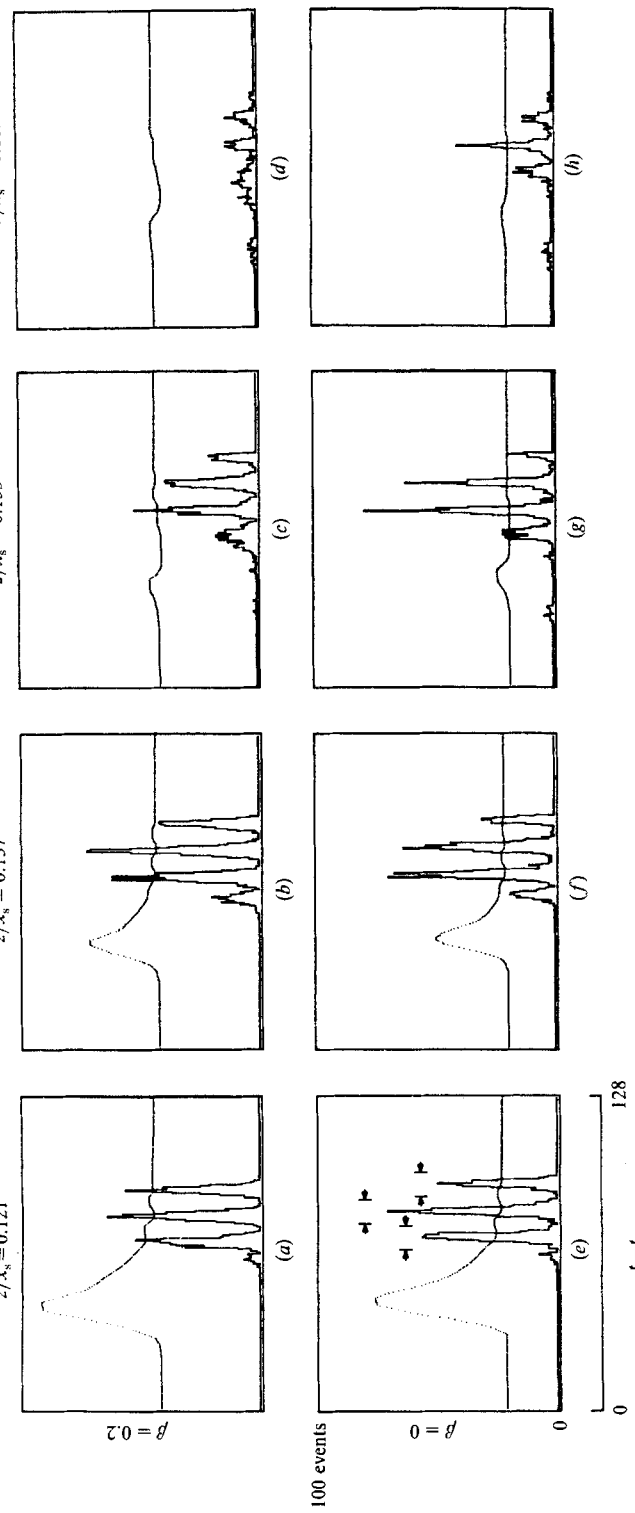

FIGURE 15. Histograms showing the number of troughs in the packet and their time of occurrence. The corresponding ensemble-averaged velocity perturbation is shown for reference.

to a frequency of 80–100 Hz) depending on the location, the waves are not lost by the averaging procedure.

The amplitude of the waves calculated from the ensemble-averaged time series deteriorates at both large and small values of z and, therefore, a different procedure is required to estimate the actual amplitude of the waves in each realization, regardless of jitter. Two and three wave crests in a packet were most common at $x_s = 620$ mm, accounting for approximately 35% of the events; but four crests occurred in at least 10% of the realizations. One may regroup the waves into numbers 1, 2, and 3 by considering a 10 ms time interval surrounding each peak in the histograms shown in figure 15. For example, in figure 15(*e*), 35% of the events fall into categories 1 and 2 each, while 25% fall into category 3. The average amplitude of these waves may be determined from this classification. One may also determine the average amplitude of waves 1–3 by considering only those wave packets in which three wave troughs have been observed. The amplitudes of the wave troughs using either calculation scheme turned out to be almost identical, *but they were quite different from the amplitudes calculated from the ensemble-averaged velocity records shown in figure 12. The amplitudes of the waves, whenever they were discernible, increased monotonically with decreasing z.* This should not be confused with turbulent intensity, which shows the opposite trend after breakdown (i.e. decreases with decreasing z; see figure 9). One may conclude that the highest amplitude of the wave occurs before breakdown and the highest amplitude of the turbulent intensity follows thereafter. Whenever there is no breakdown, the waves seem to disappear in the vicinity of the calmed region because the number of realizations in which they are observed is greatly reduced.

The stable velocity profile in the calmed region might have been the result of induction by the vortices within the spot, or it might have been a product of interacting waves which originated near the wing-tips of the spot and amalgamated while turning in the streamwise direction (figure 14). The cause of the generation of the calmed region was never determined, and the hypotheses proposed presently have yet to be proven. Nevertheless, whether the wave packet breaks down as a separate entity or interacts with the spot by generating the calmed region or, perhaps, decays according to stability considerations, it still remains part and parcel of the turbulent spot affecting, at least to some extent, the flow field in its vicinity. By assuming that the calmed region represents an induced flow field generated by the large eddies embedded in the spot, one expects the borders of this region to scale in the same manner as the borders of the turbulent spot. If, however, the calmed region is produced by the packet whose wave crests were rotated in the streamwise direction, different scaling laws will have to be applied. The present results indicate that the calmed region does not scale with x_s (i.e. the distance from the spark), which is the similarity lengthscale for the turbulent boundaries of the spot. While the boundaries of the spot collapse onto a single curve over the long distances considered (e.g. figure 12), the length of the calmed region, defined in this case by $U_{\text{pert}} = 2\%$, when plotted in the similarity coordinates, becomes significantly shorter over a distance of 40 mm (figure 16). In fact, the rate of elongation of the calmed region is equivalent to the spreading rate of the envelope of the wave packet (figure 11), which provides some circumstantial evidence that the latter may be the cause of the very existence of the calmed region.

The effects considered are intimately related to the local shape of the velocity profile and the rate of divergence of the laminar boundary layer in the direction of streaming because these two parameters govern the sensitivity of the boundary layer

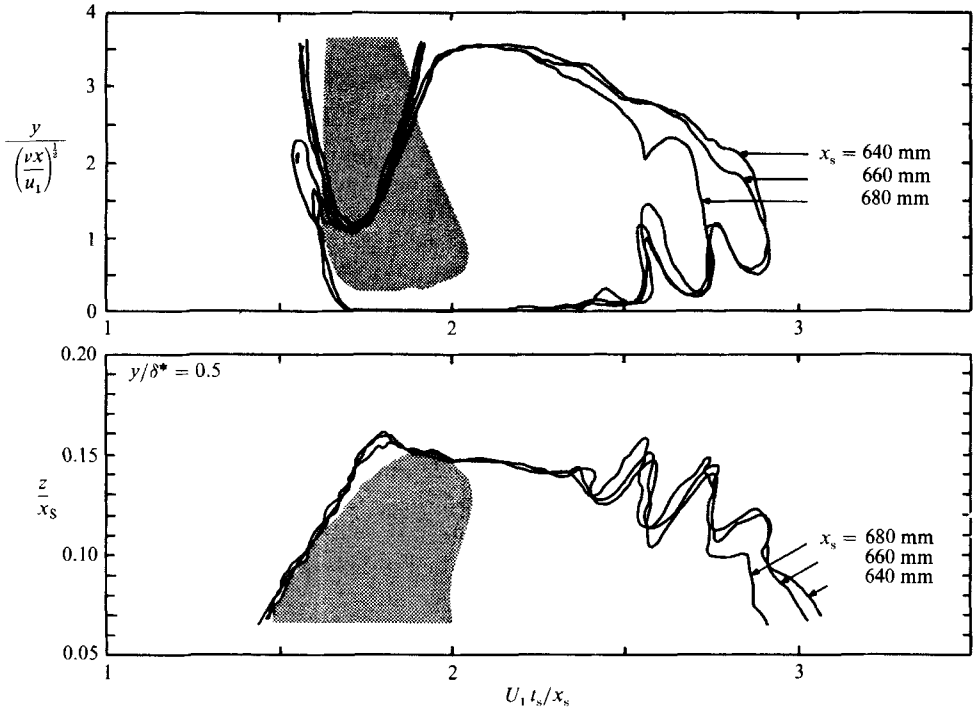

FIGURE 16. The lack of similarity in the boundaries of the 'calmed region'. The edge of the calmed region is marked by $U_{\text{pert}} = 2\%$. The shaded area indicates $\gamma > 50\%$.

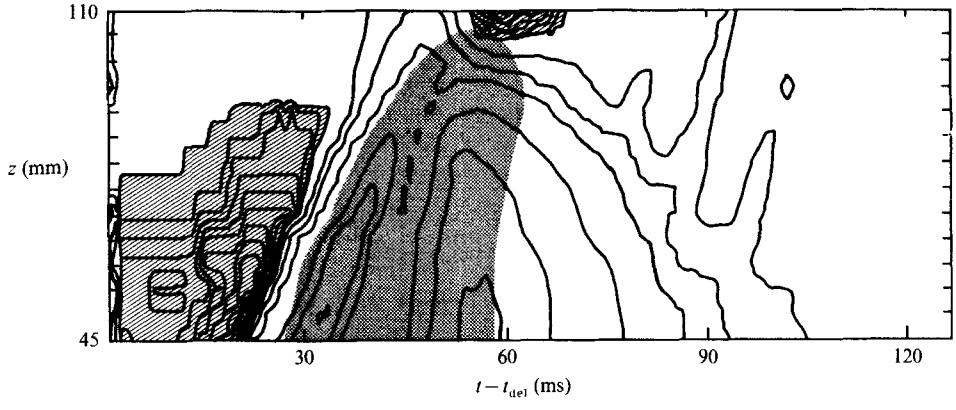

FIGURE 17. Contours of spatial amplification $(-\alpha_i \delta^*/Re_{\delta^*} \times 10^5)$ in the (z, t)-plane for $f = 96$ Hz based on data taken at $x_s = 680$ mm, $\beta = 0.2$. Contour levels are -0.5 to -3 at intervals of 0.5. The hatched areas represent an unstable flow regime. Contour levels in the hatched areas are 0 to 0.4 at intervals of 0.05. The shaded area indicates $\gamma > 50\%$.

to extraneous disturbances over which one has limited control. The relationship between the growth of the spot, the breakdown of the wave packets, and the stability of the boundary layer may be further ascertained by solving the Orr–Sommerfeld equation for spatially growing disturbances in a two-dimensional flow field, assuming that the velocity field produced by the passage of the spot describes the basic, given

state of the flow. Contours of the dimensionless amplification rate for the predominant frequency of 95 Hz at $U_1 = 11.4$ m/s during the spot passage at $x_s = 680$ mm are shown in figure 17. The boundaries of the spot at an elevation of 1 mm are also plotted by comparison. This calculation procedure may not be truly valid because (i) the perturbed flow field is three-dimensional, (ii) the boundary layer diverges quite rapidly during passage of the spot, and (iii) the possible interaction with turbulence was not considered. Nevertheless, the contours shown delineate clearly the unstable regions (represented by cross-hatched areas) which coincide with the leading interface of the spot and with the moving generator located beyond its tip. The contours corresponding to stable regions resemble the contours of the mean velocity perturbation. Consequently, the waves (which are convected downstream at a slower rate than the tip of the spot), after being amplified in the moving generator, decay as they start lagging behind the spot. Similar observations can be made for $\beta = 0$ at subcritical Re_{δ^*}. The detailed correspondence between these oversimplified calculations and the experiment are encouraging since they provide a tool for proper theoretical analysis.

3.3. *Artificial excitation of the wave packet*

It was shown that a favourable pressure gradient decreases the rate of amplification of the wave packet, thereby delaying its breakdown to turbulence. In order to confirm that the opposite argument holds true, one may either introduce an adverse pressure gradient into the flow or else retain the Blasius boundary layer ($\beta = 0$) and artificially enhance the amplitude of the wave packet trailing the spot. The latter scheme was adopted during this investigation and was implemented by an external introduction of a disturbance which, by itself, evolved into a small-amplitude wave packet but otherwise favourably interacted with the packet trailing the spot. This disturbance contributed to the increase of amplitudes of the waves within the packet and led to an earlier breakdown. This method was explored because it offers new means of controlling the transition process and may reveal some aspects of the nonlinear nature of the interaction among waves. The disturbance was generated by a short pulse in the form of a momentary jet discharging at a right angle to the surface during the passage of the low-velocity region induced by the wing-tip of the spot. The jet emerged from a static pressure hole, 0.3 mm in diameter, located at $x_s = 400$ mm and $z = 80$ mm, and was generated by a small speaker attached to the underside of the plate. The cavity behind the static hole had to be filled with foam rubber so that the pressure fluctuations associated with the passage of the spot would not trigger a cavity resonance, which in turn always interacted with the wave packet. Thus, before proceeding with the experiment, it was verified that, in the absence of the external excitation, the spot and the waves trailing it were not affected by the presence or absence of the static hole.

The amplitude of the disturbance was adjusted in such a manner that it generated a weak wave packet, in agreement with the linear stability theory over the distances considered (see Gaster & Grant 1975). When the disturbance was introduced during the passage of the spot, the amplitude of the waves in the packet trailing the spot was increased, resulting in a premature transition to turbulence. Contours of turbulent intensity measured at three streamwise locations, $x_s = 620$, 700, and 780, at $z = 80$ mm, with and without external excitation, are plotted in figure 18. The size of the turbulent patch and the level of the turbulent intensity within it are greatly increased by the excitation at $x_s = 620$ and $x_s = 700$. The external excitation caused

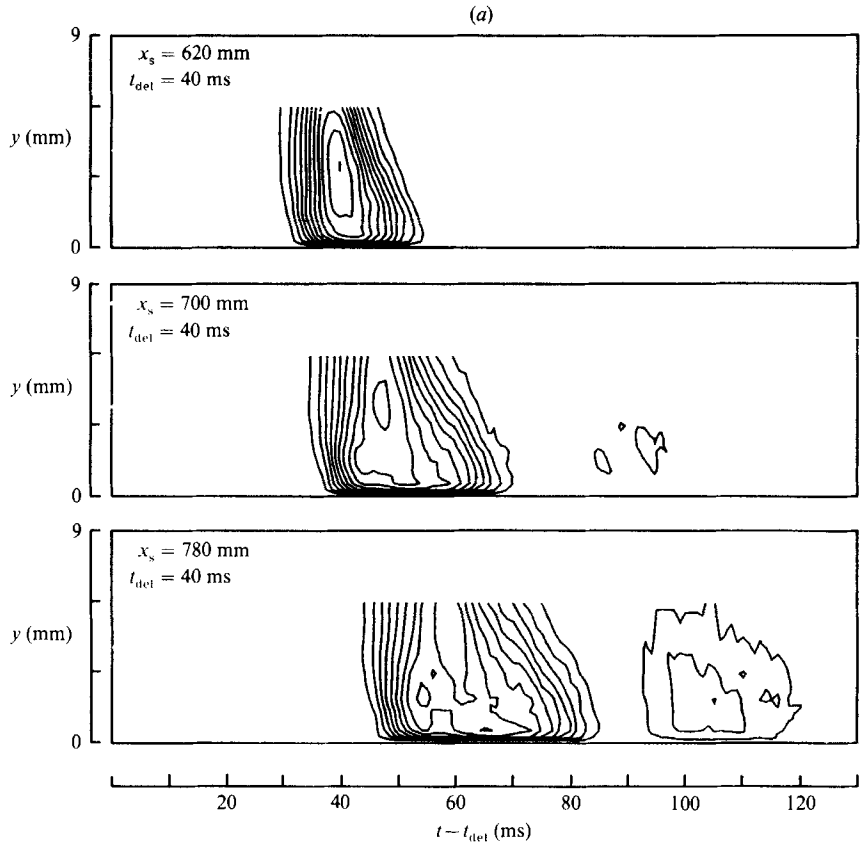

FIGURE 18(a). For caption see facing page.

transition to occur at $x_s = 620$ mm, while natural transition occurs farther downstream. The effects of the momentary excitation fade away farther downstream because the duration, and therefore the spatial extent, at which the two packets interact is limited. This experiment shows that the amplitude of the waves trailing the spot affects the location of their transition which, in turn, influences the shape and the size of the spot.

4. Conclusions

Waves emerging from the low-velocity region outside the wing-tip of the spot may amplify or decay, depending on the stability of the surrounding boundary layer. The wave packet may sometimes be a passive attendant to the turbulent spot or may be an active participant in the growth of the spot and the turbulent contamination of the laminar boundary layer. A turbulent patch generated by the breakdown of the waves increases in size while it propagates downstream, eventually amalgamating with the spot. The shape of the spot is therefore continuously changing with increasing distance from its generator because the trailing interface of the spot in a plan view becomes increasingly more concave with the passage of time. The front of the spot, acting as a large spanwise vortex, lifts off low-momentum fluid from the vicinity of the surface, actively destabilizing the boundary layer ahead of it. This

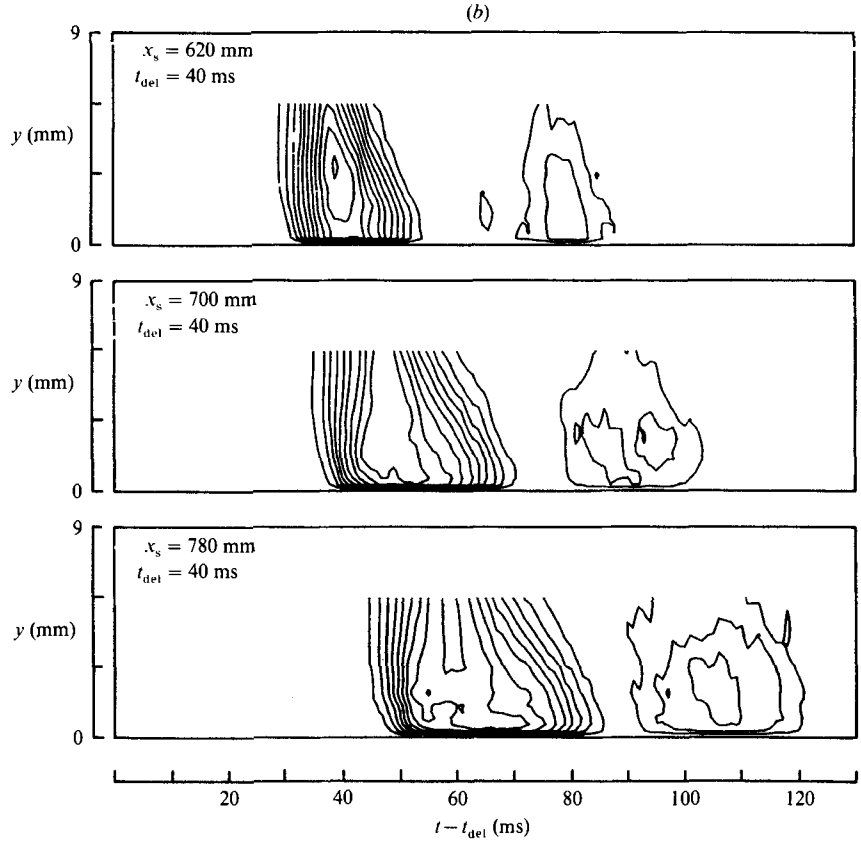

FIGURE 18. 'True' r.m.s. contours in the (y, t)-plane at $x_s = 620$ mm, 700 mm, and 780 mm, $z = 85$ mm: (*a*) unexcited; (*b*) excited.

destabilization, followed by transition, occurs so rapidly that the leading interface propagates downstream with a velocity nearly as large as the maximum velocity of the flow.

The research described in this paper was supported by the Air Force Office of Scientific Research under Grant AFOSR 84-0333.

REFERENCES

ANTONIA, R. A., CHAMBERS, A. J., SOKOLOV, M. & VAN ATTA, C. W. 1981 *J. Fluid Mech.* **108**, 317.

CANTWELL, B., COLES, D. & DIMOTAKIS, P. 1978 *J. Fluid Mech.* **87**, 641.

CHAMBERS, F. W. & THOMAS, A. S. W. 1983 *Phys. Fluids* **26**, 1160.

COLES, D. & BARKER, S. J. 1975 In *Turbulent Mixing in Nonreacting and Reacting Flows* (ed. S. N. B. Murthy), p. 285. Plenum.

CORRSIN, S. & KISTLER, A. L. 1955 Free stream boundaries of turbulent flows. *NACA Rep.* 161244.

GAD-EL-HAK, M., BLACKWELDER, R. F. & RILEY, J. J. 1981 *J. Fluid Mech.* **110**, 73.

GASTER, M. 1975 *Proc. R. Soc. Lond.* A **347**, 271.

GASTER, M. & GRANT, I. 1975 *Proc. R. Soc. Lond.* A **347**, 253.

GLEZER, A. & COLES, D. E. 1988 An experimental study of a turbulent vortex ring. *J. Fluid Mech.* (submitted).

KLEBANOFF, P. S., TIDSTROM, K. D. & SARGENT, L. M. 1962 *J. Fluid Mech.* **12**, 1.

KOVASZNAY, L. S. G., KOMODA, H. & VASUDEVA, B. R. 1962 In *Proc. Heat Transfer and Fluid Mechanics Institute*, p. 1. Stanford University Press.

MATSUI, T. 1980 In *Laminar–Turbulent Transition* (ed. R. Eppler & H. Fasel), p. 288. Springer.

MORKOVIN, M. V. 1969 Critical evaluation of transition from laminar to turbulent shear layers with emphasis on hypersonically travelling bodies. *Flight Dynamic Lab. Rep.* AFFDL-TR-68-149.

PERRY, A. E., LIM, T. T. & TEH, E. W. 1981 *J. Fluid Mech.* **104**, 387.

SCHUBAUER, G. B. & KLEBANOFF, P. S. 1956 Contributions on the mechanics of boundary layer transition. *NACA Rep.* 1289.

SCHUBAUER, G. B. & SKRAMSTAD, H. K. 1948 Laminar boundary layer oscillations on a flat plate. *NACA Rep.* 909.

VAN ATTA, C. W. & HELLAND, K. N. 1980 *J. Fluid Mech.* **100**, 243.

WAZZAN, A. R., OKAMURA, T. T. & SMITH, A. M. O. 1968 Spatial and temporal stability charts for the Falkner–Skan boundary layer profiles. DAC 67086, Sept. 1, 1968, McDonnell Douglas Corp.

WYGNANSKI, I. J. & CHAMPAGNE, F. H. 1973 *J. Fluid Mech.* **59**, 281.

WYGNANSKI, I. & FIEDLER, H. 1970 *J. Fluid Mech.* **41**, 327.

WYGNANSKI, I. J., HARITONIDIS, J. H. & KAPLAN, R. E. 1979 *J. Fluid Mech.* **92**, 505.

WYGNANSKI, I. J., SOKOLOV, M. & FRIEDMAN, D. 1975 *J. Fluid Mech.* **69**, 283.

WYGNANSKI, I. J., ZILBERMAN, M. & HARITONIDIS, J. H. 1982 *J. Fluid Mech.* **123**, 69.

ZILBERMAN, M. 1981 On the interaction of transitional spots and generation of a synthetic turbulent boundary layer. Ph.D. thesis, Tel-Aviv University.

ZILBERMAN, M., WYGNANSKI, I. J. & KAPLAN, R. E. 1976 *Phys. Fluids Suppl.* **20**, S258.